

# Leidenfrost Dynamics

David Quéré

Physique et Mécanique des Milieux Hétérogènes, CNRS UMR 7636, ESPCI, 75005 Paris, France, and Departments of Mechanics and Physics, Ecole Polytechnique, 91120 Palaiseau, France; email: david.quere@espci.fr

Annu. Rev. Fluid Mech. 2013. 45:197–215

First published online as a Review in Advance on September 27, 2012

The *Annual Review of Fluid Mechanics* is online at [fluid.annualreviews.org](http://fluid.annualreviews.org)

This article's doi:  
10.1146/annurev-fluid-011212-140709

Copyright © 2013 by Annual Reviews.  
All rights reserved

## Keywords

film boiling, levitation, nonwetting

## Abstract

This review discusses how drops can levitate on a cushion of vapor when brought in contact with a hot solid. This is the so-called Leidenfrost phenomenon, a dynamical and transient effect, as vapor is injected below the liquid and pressed by the drop weight. The absence of solid/liquid contact provides unique mobility for the levitating liquid, contrasting with the usual situations in which contact lines induce adhesion and enhanced friction: hence a frictionless motion, and the possibility of bouncing after impact. All these characteristics can be combined to create devices in which self-propulsion is obtained, using asymmetric textures on the hot solid surface.

## 1. A FEW HISTORICAL FACTS

In the second part of his famous novel *Michel Strogoff*, Jules Verne (1876) has his eponymous hero punished with blindness when his eyes are exposed to a red-hot sword. The villain who ordered this torture takes advantage of the situation, until the last chapter, when we realize, to our complete surprise, that Strogoff has only pretended to be blind—a ruse that permits his victory in the final fight against the villain. As explained by Verne, Strogoff had been saved from blindness by the insulating properties of the vapor film that formed as the hot metal approached his humid eyes. The literary history of this effect does not stop here, and probably reaches its apogee more than 30 years later, at the beginning of *Swann's Way*, in which Marcel Proust (1913) uses it in a subtle metaphor:

When I saw an external object, my awareness that I was seeing it would remain between me and it, lining it with a thin spiritual border that prevented me from ever touching directly its substance; it would volatilize in some way before I could make contact with it, just as an incandescent body brought near a wet object never touches its moisture because it is always preceded by a zone of evaporation.

The absence of contact between a liquid such as water and hot metals had been observed much earlier, probably since the dawn of metallurgy. Hot plates are most often cooled with water, and the formation of an insulating layer of vapor is of course detrimental for lowering the temperature of these plates. But it seems that the first modern observation of the phenomenon we are interested in here was by Herman Boerhaave (1668–1738) from Leiden, who reported in 1732 that alcohol poured on a hot plate does not catch fire but instead forms into “a gleaming drop resembling quicksilver” (Boerhaave 1732, experiment 19, p. 257; Curzon 1978). However, the effect was named after Johann Gotlob Leidenfrost (1715–1794) from Duisburg, who carefully described it in chapter 15 of his *Treatise on the Properties of Common Water*, published in Latin in 1756 (Curzon 1978; Leidenfrost 1756a,b). He used polished iron spoons “heated over glowing coals” and noticed that a drop of water falling into the glowing spoon “does not adhere to the spoon, as water is accustomed to do, when touching colder iron.” Leidenfrost (1756b) then noted that

the water globule will lie quiet and without any visible motion, without any bubbling, very clear like a crystalline globe, always spherical, adhering nowhere to the spoon, but touching it in one point. Although motion is not visible in the pure drop, nevertheless it delights in a very swift motion of turning, which is seen when a small colored speck, for example some black carbon, adheres to the drop. . . . Moreover, this drop only evaporates very slowly: it runs a little over half a minute before it disappears. Which at last exceedingly diminished so that it can hardly any more be seen, with an audible crack, which with the ears one easily hears, it finishes its existence. (Curzon 1978)

Placing a candle behind the drop, Leidenfrost could observe with the naked eye that light passes between the hot solid and the liquid, revealing the existence of a film of vapor below the drop.

**Figure 1a** shows this direct observation made by Leidenfrost. A millimeter-size drop of water is placed on a flat polished metallic plate at 300°C. Backlighting is used, which helps to distinguish the interval between the drop and its reflection owing to the presence of vapor. A larger drop is flattened by gravity (**Figure 1b**), but the film is also clearly visible, and its thickness, found to be of the order of 100  $\mu\text{m}$ , is indeed visible with the naked eye. A similar experiment can be made with a solid sublimating at atmospheric pressure, as solid carbon dioxide (dry ice) does (**Figure 1c**) (Lagubeau et al. 2011). Its sublimation temperature is  $-80^\circ\text{C}$ , so a piece of dry ice on the same hot solid as that in **Figure 1a,b** similarly levitates on a vapor film of comparable thickness. Leidenfrost

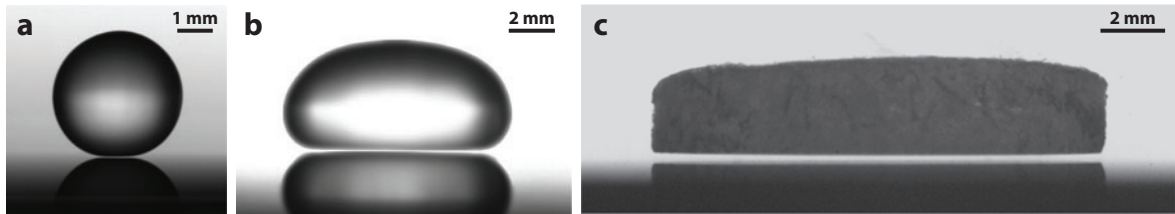


**Figure 1**

Leidenfrost bodies on a flat metallic plate at 300°C: (a) A quasi-sphere water drop, (b) a water puddle flattened by gravity, and (c) a disk of dry ice. All these materials levitate on a cushion of vapor, whose thickness is typically 100  $\mu\text{m}$ . Figure courtesy of Raphaële Th evenin and Dan Soto.

drops can also be observed on a liquid bath, provided the bath is hot enough (e.g., liquid nitrogen on water) (Snezhko et al. 2008).

A levitating liquid is extremely mobile (see **Supplemental Video 1**), so it is necessary to trap it to follow its evolution (the Leidenfrost spoon) (follow the **Supplemental Material link** from the Annual Reviews home page at <http://www.annualreviews.org>). A classical test consists of measuring the lifetime  $\tau$  of the drop as a function of the substrate temperature  $T_S$  (Gottfried et al. 1966), an example of which is shown in **Figure 2** (Biance et al. 2003). It is observed that  $\tau$  rapidly decreases as  $T_S$  approaches the boiling point (100°C for water), where it is approximately one-tenth of a second: At 100°C, water contacts its substrate, and myriads of bubbles are generated, producing the rapid disappearance of the liquid and a characteristic noise. However, the lifetime  $\tau$  dramatically increases when the plate becomes hotter: It abruptly jumps to 90 s when  $T_S$  becomes approximately 150°C. For higher temperatures, the lifetime logically decreases with  $T_S$ , but the decrease is slow: A small drop survives more than 30 s on a plate at 400°C.

 Supplemental Material

The abrupt increase of  $\tau$  corresponds to the appearance of a vapor cushion, a regime sometimes referred to as film boiling (Tong 1997). The gap insulates the liquid from its substrate and also prevents the nucleation of bubbles owing to the absence of solid/liquid contact. The critical temperature of film boiling is called the Leidenfrost temperature,  $T_L$ , and there is still some debate about its thermodynamic status (Bernardin & Mudawar 1999). We can find in the literature similar measurements done on various substrates, which show how  $T_L$  depends (or not) on the nature of the substrate (Liu & Craig 2010) and specifically on its roughness (Bernardin & Mudawar 1997). As initially noted by Leidenfrost, experiments are reproducible only with polished substrates:

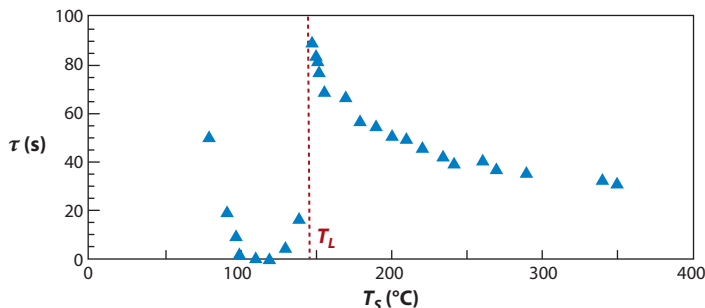


**Figure 2**

Lifetime  $\tau$  of a water droplet of radius  $R = 1$  mm as a function of the temperature  $T_S$  of the polished aluminum plate on which it is deposited. Being much smaller than 1 s at the boiling point of water, this time sharply increases at the temperature  $T_L$  for which a thick film of vapor sets between the plate and the liquid (Biance et al. 2003).

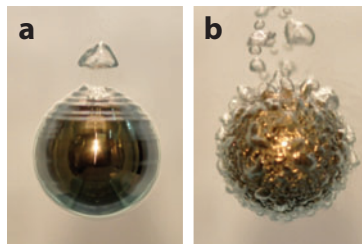


**Figure 3**

Stationary hot steel ball (diameter of 15 mm) in FC-72, a fluorinated liquid with a boiling point of 56°C. (a) For a ball temperature  $T_S$  larger than  $T_L = 130^\circ\text{C}$ , a film of vapor forms (the inverse Leidenfrost phenomenon) and drains, generating ripples and bubbles at the upper pole. (b) After 30 s, the ball's temperature reaches  $T_L$ , which produces an explosive release of bubbles. Figure taken from Vakarelski et al. (2011), courtesy of Ivan Vakarelski and Sigg Thoroddsen.

Roughness triggers the nucleation of bubbles and thus tends to increase the temperature  $T_L$ . This can be exploited to suppress the Leidenfrost effect, as shown by Weickgennant et al. (2011) who reported that polymer nanofiber mats deposited on a hot metal prevent the formation of vapor film, which considerably enhances the cooling of the (hot) plate by the incoming (cold) drops. Heat exchange is also favored for salt solutions because of the roughness induced by the salt on the solid surface (Cui et al. 2003). Conversely, having a microtextured hydrophobic surface can extend the Leidenfrost state down to the boiling point of the liquid (100°C for water), as shown by Vakarelski et al. (2012).

If a hot (smooth) object is immersed in a liquid with a much lower boiling temperature, it similarly can be surrounded by a layer of vapor. This inverse Leidenfrost effect was first described by Faraday (1828), and more recently by Hall et al. (1969), by Fletcher & Thyagaraja (1989), and by Vakarelski et al. (2011). It is visible in **Figure 3a**, which shows a centimeter-size steel ball initially at  $T_S = 250^\circ\text{C}$  immersed (and maintained magnetically) in a liquid called FC-72 (mainly perfluorohexane) at 25°C. The boiling point of FC-72 is 56°C, and a vapor film (of typical thickness 100  $\mu\text{m}$ ) is clearly visible around the ball, producing bubbles at the upper pole (Vakarelski et al. 2011). The Leidenfrost temperature  $T_L$  here is 130°C; after half a minute, this temperature is reached so that the ball contacts the liquid, which produces an explosive boiling (**Figure 3b** and **Supplemental Video 2**). These inverse Leidenfrost situations also exist for liquid/liquid systems: If placed on a “cold” liquid, a “hot” drop can float because of the vapor film. Song et al. (2010) proposed the use of this experiment to vitrify liquid (e.g., water on a bath of liquid nitrogen).

## 2. SHAPE AND STABILITY OF LEIDENFROST DROPS

### 2.1. Shape of the Drops

A Leidenfrost drop is in a nonwetting situation: A liquid completely dewets a substrate covered with vapor, which it meets with an angle of 180°. More generally, Young's relationship,  $\cos\theta = (\gamma_{SV} - \gamma_{SL})/\gamma_{LV}$ , relates the contact angle  $\theta$  of a liquid on a solid to the different surface tensions  $\gamma_{IJ}$  (the indices  $S$ ,  $L$ , and  $V$  refer to the solid, liquid, and vapor, respectively) (Young 1805). On a vapor substrate, we can replace the index  $S$  by  $V$  in the formula, which indeed yields  $\theta = 180^\circ$ . The only surface tension involved in a Leidenfrost drop is thus the liquid/vapor one, which we denote as  $\gamma$ .

This nonwetting property implies that small drops are quasi-spheres (**Figure 1a**), whereas larger ones become flattened by gravity (**Figure 1b**). Such puddles can be approximated to the first order by disks of equatorial radius  $R$  and thickness  $H$ . The transition between spheres and pancakes

occurs when the gravitational energy of a sphere, which scales as  $\rho g R^4$  (where  $\rho$  is the liquid density and  $g$  the acceleration of gravity), becomes larger than its surface energy, of order  $\gamma R^2$ . We classically find that gravity can be (nearly) neglected if the drop radius is smaller than the capillary length  $\ell_c = (\gamma/\rho g)^{1/2}$ . In a Leidenfrost situation, the temperature inside the liquid sets at the boiling point after a short transient time so that the quantities  $\gamma$  and  $\rho$  are known for a given liquid. For water, for example, we have  $\gamma = 59 \text{ mN m}^{-1}$  and  $\rho = 960 \text{ kg m}^{-3}$ , which give  $\ell_c = 2.5 \text{ mm}$ .

Let us describe more precisely the two families of shapes observed in **Figure 1a** ( $R < \ell_c$ ) and **Figure 1b** ( $R > \ell_c$ ). At equilibrium, the Laplace pressure  $\gamma\kappa$  (with  $\kappa$  the curvature of the interface) is balanced by the hydrostatic pressure  $\rho g(H - z)$ , where  $z$  is the vertical coordinate starting from the plate. This equation for the shape can be rewritten  $\kappa = \kappa_o + (H - z)/\ell_c^2$ , where we introduce the top curvature  $\kappa_o$ . On the one hand, small drops are quasi-spheres of radius  $R$ , of curvature  $\kappa_o \approx 2/R$  and height  $H \approx 2R$ . On the other hand, the top of a puddle is nearly flat ( $\kappa_o \approx 0$ ), and the shape equation  $\kappa \approx (H - z)/\ell_c^2$  is the same as that for a meniscus in cylindrical coordinates. The curvature increases linearly along the interface as we go from the top ( $z = H, \kappa = 0$ ) to the bottom ( $z = 0, \kappa = H/\ell_c^2$ ) (**Figure 1b**). Integrating analytically, the shape equation yields the thickness of a nonwetting gravitational pancake,  $H = 2\ell_c$ . This value can also be derived from the energy  $F$  of a puddle, the sum of a gravitational and a surface term. For  $R \gg \ell_c$ , the energy can be written  $F \approx \pi \rho g R^2 H^2/2 + 2\pi \gamma R^2$ . Minimizing  $F$  at constant volume  $\Omega \approx \pi R^2 H$  brings us back to  $H \approx 2\ell_c$ . Passing from a small drop to a large one, the liquid height  $H(R)$  thus first increases as  $2R$  (for  $R < \ell_c$ ) before saturating at  $2\ell_c$  (for  $R > \ell_c$ ) (Biance et al. 2003). This maximum height is strictly not valid when the drop size is just above the capillary length. The Laplace pressure associated with the equator curvature tends to squeeze the liquid, resulting in a thickness slightly larger than  $2\ell_c$ . As shown numerically, the maximum thickness is expected for  $R \approx 3.2\ell_c$ , where it is  $H \approx 2.1\ell_c$  (Aussillous & Quéré 2006).

Small drops are also somehow flattened by gravity, but only close to the plate (**Figure 1a**) (Mahadevan & Pomeau 1999). We denote as  $\ell$  the radius of the flat region below the drop. Although we are in the limit  $R < \ell_c$ , a small deformation  $\delta$  of a sphere of radius  $R$  contacting a nondeformable plate induces an appreciable “contact.” From elementary geometry, we obtain  $\ell \sim (\delta R)^{1/2}$ , which critically increases at small  $\delta$ . The deformation  $\delta$  results from the drop weight  $\rho g R^3$ , and it is resisted by an elastic force  $\gamma \delta$ . Hence a vertical deformation  $\delta$  is approximately  $R^3/\ell_c^2$ , and a lateral contact  $\ell$  scales as  $R^2/\ell_c$  (Mahadevan & Pomeau 1999). This result can be recovered (with its numerical coefficient) by assuming a flat interface below the drop. The pressure there is  $4\rho g R^3/3\ell^2$ , which is also obtained by crossing this flat interface from inside the drop, of internal pressure  $2\gamma/R$ . The quadratic law of contact  $\ell \sim R^2/\ell_c$  is very different from what holds for a wetting drop, for which it increases linearly with the drop size ( $\ell \sim R \sin \theta$ ). It implies in particular that the smaller the drop is, the larger the (Laplace) pressure  $2\gamma/R$  exerted on the subjacent film—because of this divergence, a Leidenfrost drop will contact (only) its hot substrate at the moment it vanishes (so to speak)!

We used only static arguments above, although both the liquid and vapor move: As noted by Leidenfrost himself, convection takes place inside the drop (of viscosity  $\eta$ ) (Snezhko et al. 2008), and the vapor film (of viscosity  $\eta_v$ ) escapes laterally, pressed by the liquid. These flows may influence the shape of the drop (as seen below) but quite marginally in general. Flow inside the drop can be caused by different factors. For example, liquid is drawn by the moving vapor: Balancing the viscous stress in the film  $\eta_v U/b$  with the viscous stress in the drop  $\eta V/R$ , one yields a typical velocity  $V \sim U(R/b)(\eta_v/\eta)$ , that is, approximately  $1 \text{ cm s}^{-1}$  for a vapor velocity  $U = 10 \text{ cm s}^{-1}$  and a film thickness  $b = 100 \text{ }\mu\text{m}$  (as evaluated further below). It was also reported that the temperature in the liquid decreases by a few degrees from the film, where it is at the boiling point, to the top (Bouasse 1924, chapter 7; Tokugawa & Takaki 1994), which generates Marangoni

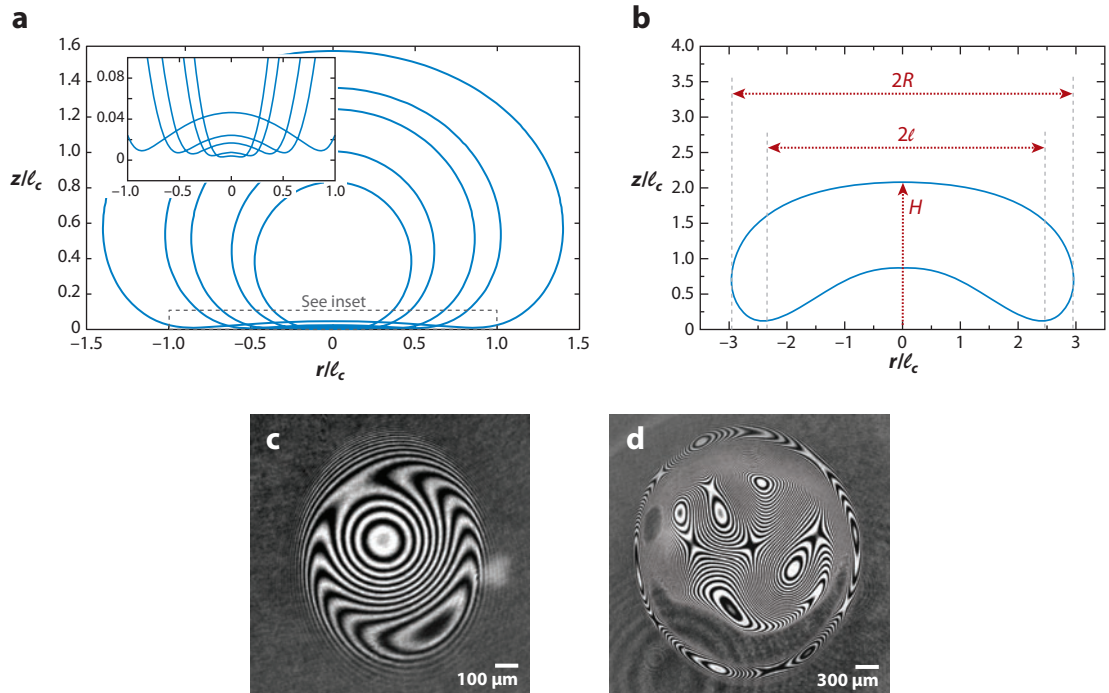


**Figure 4**

Stable Leidenfrost drops. (a,b) Numerical simulations showing a vapor pocket [whose height increases with drop size (see the *inset* in panel a)] forming below the drop of profile  $z(r)$ . Here the film is made by airflow normal to the substrate below the drop, and the scale is given by the capillary length  $\ell_c$ . (c,d) Direct interferometric measurements from below confirm the existence of these pockets, whose profiles are more complex if the drop is larger. Panels a and b taken from Snoeijer et al. (2009), courtesy of Jacco Snoeijer, Philippe Brunet, and Jens Eggers. Panels c and d taken from Burton et al. (2012), courtesy of J. Burton and S. Nagel.

flows. A typical Marangoni velocity  $V$  in the liquid is found by balancing the viscous stress  $\eta V/R$  with the gradient of surface tension  $\Delta\gamma/R$  along the drop, which yields  $V \sim \Delta\gamma/\eta$ , typically  $10 \text{ cm s}^{-1}$  in water for  $\Delta\gamma \approx 10^{-4} \text{ mN m}^{-1}$ , a value corresponding to a temperature difference of a few degrees. This indeed is a correct order of magnitude for the liquid velocity inside a Leidenfrost drop. The corresponding Weber and capillary numbers are thus small compared to unity, which demonstrates that surface tension maintains a static shape despite the presence of these flows.

## 2.2. At the Liquid/Vapor Interface

In this section we discuss the shape of the underlying liquid/vapor interface. This interface is assumed above to be flat for small drops ( $R < \ell_c$ ), which becomes questionable if the drop is larger than  $\ell_c$ , that is, if the Archimedes thrust on the gas film is stronger than the action of surface tension. In this limit, we expect to see a pocket of vapor below the drop with a similar shape (yet upside down) to the one of a wetting drop of the same size hanging from a ceiling (Biance et al. 2003, Snoeijer et al. 2009). This shape can be stationary if the drop radius is not too large, as in **Figure 4a,b**, which shows the calculated profiles of drops smaller and larger than  $\ell_c$ , together with a close-up of the “contact” region (Snoeijer et al. 2009). Burton et al. (2012) directly observed

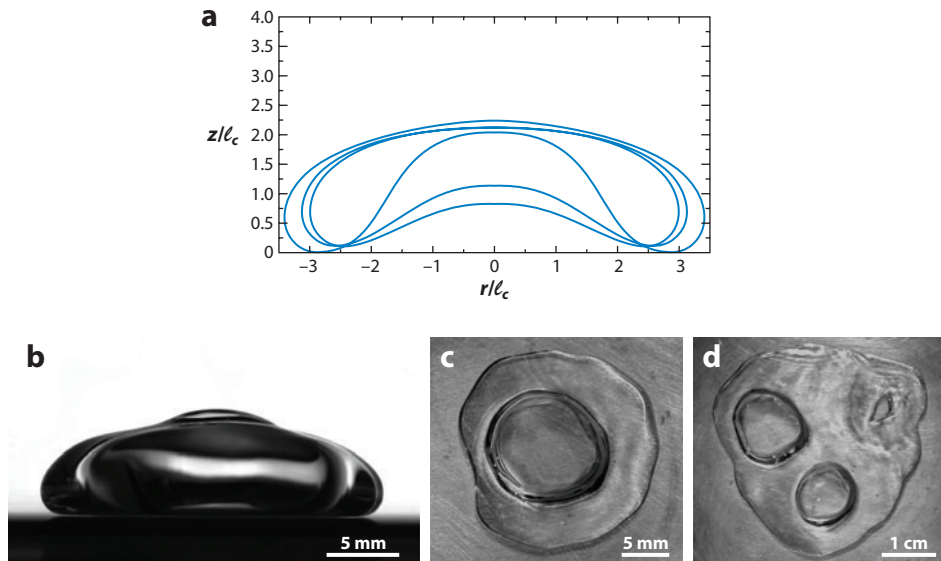


**Figure 5**

Very large Leidenfrost drops not only are flattened by gravity, they are also unstable, and a chimney of vapor forms at the center and rises. Simulations show that the critical size is dictated by a balance between the surface tension and gravity, with a correction related to the vapor flow. (a) Successive profiles of the vapor pocket rising in the liquid. (b) The chimney makes a dome at the top of the liquid. (c,d) From above, the chimneys become evident. Panel a taken from Snoeijer et al. 2009, courtesy of Jacco Snoeijer, Philippe Brunet, and Jens Eggers. Panel b courtesy of Raphaële Thévenin and Dan Soto. Panels c and d taken from Biance et al. (2003), courtesy of Anne-Laure Biance.

these zones by looking at water drops on hot transparent surfaces (sapphire) from below. Using light interferences (Figure 4c,d), they showed that the concave depressions become increasingly marked and complex as the drop size increases around the capillary length.

The vapor cavity can become unstable for larger drops (Figure 5). Then the gas forms a chimney, rising at the center of the puddle and making (transiently) a dome at its top (Figure 5b) (Biance et al. 2003). Next the dome bursts, which leaves a liquid torus that closes, generating strong oscillations before a new chimney forms (see Supplemental Video 3). Similar instabilities were predicted for large puddles levitating on air-blown porous materials (Lister et al. 2008), which are analogs of the Leidenfrost phenomenon in which the role of temperature is played by the gas flux (Goldshtik et al. 1986).

This instability is easier to observe from the top (Figure 5c and Supplemental Video 4), and it is a kind of inverse Rayleigh–Taylor instability (Biance et al. 2003). Instead of having a dense film on a ceiling destabilizing downward (Taylor 1950), here we have a light film of gas destabilizing upward. Gravitational force dominates the surface tension when the radius  $\ell$  of the “contact” (defined in Figure 4b) is larger than a threshold  $\ell^*$  ( $\ell^*$  scales as the capillary length and is found in cylindrical coordinates to be  $3.8\ell_c$ ). The corresponding critical radius  $R^*$  is  $4.3\ell_c$  (Snoeijer et al. 2009), in good agreement with observations (Biance et al. 2003). This first-order approach ignores the flow of vapor below the drop, which, as shown by Snoeijer et al. (2009), slightly modifies the critical radius of destabilization. As the flow increases,  $R^*$  slowly decreases (the correction scales as the flux of vapor to the power 1/10), which can be interpreted as an effect of the lubricating pressure that favors the formation of the cavity. The

 Supplemental Material

case of even larger drops, a few centimeters or more (see **Figure 5d**), is also of interest: Multiple chimneys form with a preferential distance, such as in the Rayleigh-Taylor instability (Biance et al. 2003). The details of this situation remain to be studied, as well as the interactions between these chimneys (which close and open regularly, as mentioned above). Variations of the shape of the substrate (either solid or liquid) can also impact the instability (Lister et al. 2008, Perrard et al. 2012).

### 2.3. In the Vapor

Compared to usual liquid lenses, a unique feature of Leidenfrost drops is that they both produce vapor (on which they levitate) and press on it (which might affect the levitation). These antagonistic actions set the stationary thickness  $\varepsilon$  of the vapor film (Biance et al. 2003, Gottfried et al. 1966, Myers & Charpin 2009, Wachters et al. 1966). It is indeed crucial to understand the characteristics of the film to predict the heat transfer between the solid and the liquid, a quantity of obvious practical interest (Bernardin & Mudawar 1997, 2007), and the rate of evaporation of the liquid (Strotos et al. 2008). Let us consider a drop with a size comparable to the capillary length  $\ell_c$ , for which the bottom interface is reasonably flat, and the shape comparable with that of a disk of radius  $R$  and thickness of order  $\ell_c$ .

Conduction in the vapor gap is generally the main mechanism of heat exchange between the solid and the liquid (Avedisian & Koplík 1987, Gottfried et al. 1966). The corresponding heat flux per unit area can be written as  $\kappa(T_S - T_B)/b = \kappa \Delta T/b$ , where  $\Delta T = T_S - T_B$  is the temperature difference between the solid and the boiling point of the liquid, and  $\kappa$  is the thermal conductivity of the vapor. [The radiation heat flux per unit area is given by Stefan's law,  $\sigma(T_S^4 - T_B^4)$ , where  $\sigma$  is Stefan's constant. The ratio between radiative and convective fluxes at approximately 300°C thus can be estimated to be typically 5%. Both fluxes become comparable above 1,000°C, which justifies the assumption of a conduction-dominated heat flux at lower solid temperatures.] Hence we deduce the mass of liquid  $\dot{M}$  evaporated per unit time. After a short time to raise the liquid temperature up to  $T_B$ , we simply have  $L\dot{M} \sim (\kappa \Delta T / b)R^2$ , with  $L$  the latent heat of evaporation.

The film thickness  $b$  in the latter equation is unknown, and we need a second equation to determine  $b$  and  $\dot{M}$ . As mentioned above, the liquid squeezes the subjacent film and forces it to escape laterally. The geometry is that of a thin and long slot (typical orders of magnitude in **Figure 1b** are a few millimeters for the length and 0.1 mm for the thickness), which naturally sets the conditions of the lubrication approximation: Vapor escapes with a Poiseuille flow (assuming a no-slip condition on both solid and liquid interfaces). We deduce a scaling relationship between the vapor flux and the pressure gradient  $\nabla P$  responsible for the flow:  $\dot{M} \sim (\rho_v R b^3 / \eta_v) \nabla P$ , which introduces the vapor density  $\rho_v$  and viscosity  $\eta_v$ . The puddle applies a hydrostatic pressure of order  $\rho g \ell_c$  on the film, from which we deduce a flux  $\dot{M} \sim (\rho_v b^3 / \eta_v) \rho g \ell_c$ . In stationary conditions, the film is fed by evaporation at the rate at which vapor escapes, which yields a law for the film thickness,  $b \sim (Rb)^{1/2}$ , where the distance  $b$  scales as  $(\kappa \Delta T \eta_v / L \rho_v \rho g \ell_c)^{1/2}$  (Biance et al. 2003, Gottfried et al. 1966). Taking typical values for the different parameters ( $\kappa \approx 0.03 \text{ W m}^{-1} \text{ K}^{-1}$ ,  $\eta_v \approx 2 \times 10^{-5} \text{ Pa}\cdot\text{s}$ ,  $L \approx 10^6 \text{ J kg}^{-1}$ ,  $\rho_v \approx 1 \text{ kg m}^{-3}$ , and  $\rho \approx 10^3 \text{ kg m}^{-3}$ ), we find  $b \approx 3 \text{ }\mu\text{m}$ , which, for radii  $R$  of a few millimeters, yields a vapor thickness  $b$  of the order of 100  $\mu\text{m}$ .

These expressions allow us to evaluate the quantity of vapor produced per unit time  $\dot{M} \sim (\kappa \Delta T / bL) R^2 \sim (\kappa \Delta T / L b^{1/2}) R^{3/2}$ , typically of the order of 1 mg s<sup>-1</sup>. Assuming that the drop mainly evaporates by its bottom, this provides an estimate of the lifetime  $\tau \sim M / \dot{M}$  of Leidenfrost drops of initial mass  $M$ , that is, 100 s for puddles of a few millimeters ( $M \approx 100 \text{ mg}$ ). Note that puddles covered by a thin film of aluminum evaporate as quickly as free puddles, confirming that the bottom evaporation is dominant. The mean vapor velocity  $U$  can also be deduced from these

considerations. We have  $\dot{M} \approx 2\pi R b \rho_v U$ , from which we evaluate a velocity  $U$  of a few tens of centimeters per second, in agreement with observations (Dupeux et al. 2011b). The Reynolds number  $Re \approx \rho_v b^2 U / R \eta_v$  comparing inertial and viscous effects in the film is thus found to be of order 0.1, justifying a posteriori the dominant role of viscous forces in the vapor film. This first-order approach can be easily transposed to the case of levitating solids (**Figure 1c**), for which the thickness  $H$  of the material can be tuned independently of radius  $R$ .

Evaporation depends on the size of the system ( $\dot{M} \sim R^{3/2}$ ,  $b \sim R^{1/2}$ ), and the latter law implies that the materials slowly sink in the vapor film as they evaporate (Biance et al. 2003). For a liquid, these laws are affected when gravity becomes negligible ( $R < \ell_c$ ) (Biance et al. 2003, Bleiker & Specht 2007, Celestini et al. 2012), in particular because of the change of geometry for the contact and for the drop shape, as seen in **Figure 1a** and discussed in Section 2.1. A convenient way to test these laws is to feed Leidenfrost drops with a given flux of liquid (using a syringe placed at the top surface): After a short transient regime, this flux fixes the drop radius, from which the relationship  $\dot{M}(R)$  is immediately deduced (and found to be in good agreement with the scaling law  $\dot{M} \sim R^{3/2}$ ). If a laser beam passes below the drop, one can use the diffraction pattern to measure the film thickness. This also confirms the scaling law derived above ( $b \sim R^{1/2}$ , for  $R > \ell_c$ ) (Biance et al. 2003, Wachters et al. 1966). It is remarkable that the shape variations of the bottom interface discussed in Section 2.2 do not seem to notably modify this naïve picture. Feeding the liquid with itself can also be achieved when considering the impact of a jet on a hot solid, for which one can also observe the Leidenfrost phenomenon—this cooling device is analyzed by Gradeck et al. (2011) and Karwa et al. (2011). Finally, the conduction equation at very short time  $t$  (for which the Poiseuille flow can be neglected), that is,  $\dot{M} \sim (\kappa \Delta T / L b) R^2 \sim \rho_v \dot{b} R^2$ , suggests that  $b$  should grow with time  $t$  as  $(\kappa \Delta T t / L \rho_v)^{1/2}$ . If extrapolated to the final thickness estimated above, this law implies a very short time for the construction of the vapor film (smaller than 1 ms) (Myers & Charpin 2009), but these transient regimes remain to be studied.

### 3. SPECIAL DYNAMICS

The absence of a contact line around a levitating drop makes it “adhering nowhere,” as noted by Leidenfrost himself, and it generates original dynamical behaviors, which are also observed in superhydrophobic situations (for which the film-boiling case can be seen as a limit in terms of hydrophobicity). These drops move nearly without friction (Dupeux et al. 2011a), and they bounce when impacting solids (Biance et al. 2006, Karl & Frohn 2000, Wachters & Westerling 1966). This section discusses some of these special dynamics. The production of vapor also generates special effects, such as self-oscillations (Leidenfrost stars) (Adachi & Takaki 1984, Snezhko et al. 2008, Strier et al. 2000, Takaki & Adachi 1985, Tokugawa & Takaki 1994, Wachters et al. 1966), recently discussed in a short review by Brunet & Snoeijer (2011). In addition, the vapor ejection can be exploited to create self-propulsion (Linke et al. 2006), which we describe in Section 3.3.

#### 3.1. Friction

If we pour liquid nitrogen on the floor, the resulting drops would glide very large distances, most often comparable to the size of the room (a few meters) where the experiment was performed. The drops sweep the dust present on the floor, an effect often referred to as the lotus effect (Barthlott & Neinhuis 1997) and that takes advantage of the ability of interfaces to trap solid particles. Curiously, it appears there are no comprehensive studies in the literature devoted to these frictionless motions, maybe because of the simplicity of the friction laws expected in this

limit. We can distinguish two main causes for the friction: (a) viscous friction in the vapor film and (b) inertial friction in air. The details of the corresponding laws depend on the shape of the liquid, and for simplicity we consider here relatively large drops of thickness  $\ell_c$  and radius  $R$  ( $R > \ell_c$ ). It is easy to show that our conclusions still hold in the limit of smaller volumes of liquid.

The contact area  $\ell^2$  for  $R > \ell_c$  is comparable to the surface area  $R^2$  so that the viscous friction  $F_v$  for a liquid gliding at a velocity  $V$  scales as  $(\eta_v V/b) R^2$ , for which the vapor thickness  $b$  was evaluated in Section 2.3. Hence this friction is typically 1  $\mu\text{N}$  for a velocity of 1  $\text{m s}^{-1}$ , that is, approximately 0.1% of the drop weight. This is very different from liquids on common substrates, for which pinning forces are comparable to the weight (sticking the drops to tilted plates) and for which viscous forces opposing the motion of liquid lenses at such velocities can be even larger, also because of the existence of contact lines (Snoeijer & Andreotti 2013).

In general, the main force resisting the motion of levitating drops is the inertia of air, as it is for a raindrop. This force,  $F_i$ , scales as  $\rho_v V^2 R \ell_c$ , which typically is 10  $\mu\text{N}$ , 10 times larger than  $F_v$ . [For drops smaller than the capillary length, this hierarchy remains the same. As discussed in Section 2.1, the contact zone  $\ell$  then quickly vanishes with  $R$ , as does the force  $(\eta_v V/b)\ell^2$ .] Balancing  $F_i$  with the weight  $Mg \sin \alpha$  for a liquid running down a solid tilted by an angle  $\alpha$  relative to the horizontal direction, we obtain a final velocity  $V \sim (\rho R g \sin \alpha / \rho_v)^{1/2}$ , typically a few meters per second. Conversely, if we throw drops of liquid nitrogen on the floor, they will decelerate until friction stops them. The corresponding distance  $L$  is given by Newton's equation  $MV^2/L \sim F_i$ , from which we get  $L \sim \rho R / \rho_v$ , that is, a few meters, as mentioned above. These distances are so large that the time  $L/V$  to stop is often of the order of (or even smaller than) the evaporation time  $\tau$  evaluated in Section 2.3!

Frictionless motion can be detrimental if one tries to cool down a hot plate by using drops impacting it, or running along it. Therefore, it is worth thinking of ways to increase this friction and to promote trapping, which can be done by creating texture in the solid surface. As mentioned above, a fine hydrophilic texture (at the scale of 0.1–10  $\mu\text{m}$ ) considerably increases the Leidenfrost temperature (Kim et al. 2009, 2010; Vakarelski et al. 2012). Defects can cool close to the liquid, and thus contact it, and generate boiling (Kim et al. 2011), which of course helps to remove heat and should also modify the friction law for mobile drops. But the texture can also be much larger, comparable to the liquid scale (0.1–1 mm). When a levitating drop meets a series of crenulations placed in its way, it decelerates on centimeter-size distances instead of meters (**Figure 6** and **Supplemental Video 5**) (Dupeux et al. 2011a).

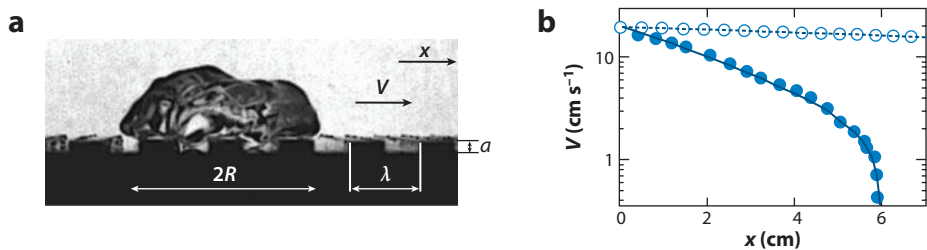


**Figure 6**

(a) Leidenfrost drop running on a plate with crenulations. (b) The drop slows down on centimeter-size distances (*solid dots*), instead of meters on a flat solid (*white dots*). This enhanced friction is attributed to the successive (soft) impacts of the bumps below the drop onto the side of the crenulations. The distance  $\lambda$  between two crenels is 1.5 mm, and their depth  $a$  is 250  $\mu\text{m}$ . Figure taken from Dupeux et al. (2011a), courtesy of Guillaume Dupeux and Marie Le Merrer.

This strong effect has been proposed to result from the successive impacts of the liquid on the crenel sides (Dupeux et al. 2011a). The liquid deforms in crenelations, and as the drop slides (and provided that it slides and does not roll), each bump hits the side of the crenel without contacting it (no boiling is observed). As known from the impact literature (Karl & Frohn 2000), normal shocks are most often soft, despite the absence of an obvious source of dissipation (such as contact lines). Kinetic energy is transferred in vibrations that later decay owing to the liquid viscosity (Biance et al. 2006). This method of slowing down a drop is efficient because it involves the liquid density, instead of the vapor density, on a flat solid. For crenelations of depth  $a$  and distance  $\lambda$ , we have  $R/\lambda$  crenels below the liquid, and each step is hit on a surface area  $Ra$ —hence an inertial “friction” force scaling as  $\rho V^2 R^2 a/\lambda$ , larger than the friction force in air by a factor  $\rho a/\rho_v \lambda$  of order 100 for  $a \approx 0.1\lambda$ . More precisely, balancing this inertial friction with the drop deceleration  $MdV^2/dx$  provides an exponential decrease of the velocity along the direction  $x$  of motion, with a characteristic length  $L = aR/\lambda$ , instead of  $\rho R/\rho_v$  on a flat solid. These exponential regimes are visible in **Figure 6** and are followed by an abrupt trapping in the crenels, possibly owing to gravity (Dupeux et al. 2011a).

The situation is even more spectacular in the inverse Leidenfrost situation, in which a hot solid in a liquid is surrounded by a film of vapor (**Figure 3a**) (Vakarelski et al. 2011). Because of the insulating properties of vapor, the Leidenfrost situation lasts long enough to study the fall of these dense hot solids in liquid and to compare the dynamics with that of a colder ball, that is, without film. We would expect an effect at small Reynolds number (but in this limit, small solids cannot stay long in the Leidenfrost state): With the solid/liquid interface (with a no-slip condition) replaced by a liquid/vapor interface, in which slip is possible (Ou et al. 2004), the factor  $6\pi$  in Stokes’s formula becomes  $4\pi$ , smaller by 50%. In Vakarelski’s experiments, the steel balls are centimeter-size, and they fall in FC-72 (see **Figure 3**), a fluorinated liquid of density  $\rho = 1,680 \text{ kg m}^{-3}$  and viscosity  $\eta = 0.64 \text{ mPa}\cdot\text{s}$ . The terminal fall velocity is a few meters per second, which corresponds to Reynolds numbers,  $Re$ , of the order of  $10^4$  to  $10^5$  (Vakarelski et al. 2011). The inertial friction  $F_i$  is then expected to be of the form  $\pi C_D \rho V^2 R^2/2$ , where we introduce the dimensionless drag coefficient  $C_D$  in the usual way. Balancing this friction with the drop weight  $4\pi \Delta \rho g R^3/3$  ( $\Delta \rho = \rho_s - \rho$ ) provides the terminal velocity of fall  $V \approx (8\Delta \rho g R/3 C_D)^{1/2}$ , apparently independent of the presence of a vapor film (which hardly modifies the apparent weight of the ball). However, results clearly show an effect, as in **Figure 7**, which illustrates the terminal velocity of a centimeter-size steel ball falling in FC-72 as a function of the ball’s temperature.

It is observed that the presence of vapor around the sphere (for  $T > T_L$ ) strongly increases the descent velocity, by a factor larger than 2 (see also **Supplemental Video 6**). As shown by Vakarelski et al. (2011), the drag coefficient  $C_D(Re)$  continuously decreases from its classical value  $C_D = 0.45$  measured at  $Re = 10^4$  to  $C_D = 0.07$ , the value at which it saturates for  $Re > 10^5$ . The vapor film modifies the shape of the wake, and the flow separation occurs close to the upper pole (because of the change of boundary condition at the sphere surface), which modifies the pressure distribution around the solid and thus the drag. The amplitude of the drag reduction is similar to that observed for the transition from subcritical to supercritical Reynolds numbers, demonstrating how efficiently vapor films decrease the friction of solids in this common range ( $10^4$ – $10^5$ ) of Reynolds numbers.

### 3.2. Impacts

Another class of dynamical questions is the impact of liquids on hot plates. It is observed that drops spread after impact, reach a maximum diameter, possibly form a torus (Biance et al. 2011), and recoil before bouncing off the plate if they are not too large ( $R < \ell_c$ ) (Bernardin et al. 1997a;

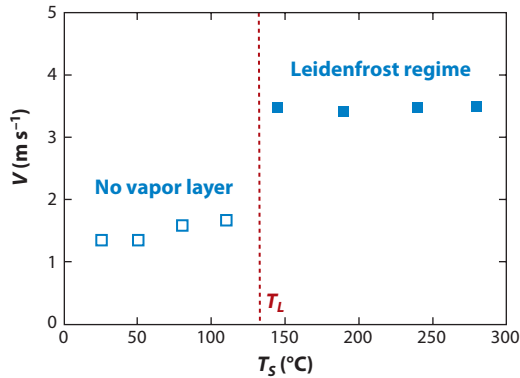


**Figure 7**

Terminal velocity of a steel ball ( $R = 1$  cm) falling in a fluorinated liquid of viscosity  $\eta = 0.64$  mPa·s, as a function of the ball's temperature  $T_S$ . The velocity becomes slightly larger above the boiling point  $T_B = 56^\circ\text{C}$ , and it suddenly increases (by a factor larger than 2) above the Leidenfrost point  $T_L = 130^\circ\text{C}$ . Figure taken from Vakarelski et al. (2011), courtesy of Ivan Vakarelski and Sigg Thoroddsen.

Biance et al. 2006; Ge & Fan 2005; Harvie & Fletcher 2001a,b; Karl & Frohn 2000; Wachters & Westerling 1966). In many cases, fragments are ejected during these phases, in particular if roughness is present (Bernardin et al. 1997a,b; Biance et al. 2011; Cossali et al. 2008; Karl & Frohn 2000; Moita & Moreira 2007). What matters in the different steps of an impact is the Weber number,  $We = \rho V^2 R / \gamma$ , which compares the kinetic energy of the incoming liquid with its surface energy. All the different characteristics evoked above (e.g., maximal diameter, onset of fragmentation, elasticity of the impact) are functions of  $We$ . There are still debates about the nature of these functions. For example, it is tempting to assume energy conservation for Leidenfrost impacts (for which viscous dissipation is highly reduced) (Chandra & Avedisian 1991). This leads to a simple prediction for the maximum radius (such that the sum of the surface and kinetic energy of the drop is stored in deformation), but this prediction is often contradicted by experiments (Biance et al. 2006, Karl & Frohn 2000, Tran et al. 2012). As a more obvious contradiction, a drop impinging a hot substrate at a velocity  $V$  generally takes off at a velocity  $V'$  significantly smaller than  $V$ : The elasticity  $V'/V$  of the shock decreases with  $We$ , passing from a value close to 1 for  $We < 1$  to values close to zero at high  $We$  (see **Supplemental Videos 7 and 8**) (Biance et al. 2006, Karl & Frohn 2000). This results from the transfer of kinetic energy to vibration energy as the drop recoils: The higher  $V$  is, the larger is the deformation at impact, and thus the stronger the vibrations are of the liquid. These energy losses (mentioned in Section 3.1) remain to be quantitatively understood.

These different behaviors concern nonwetting situations at large. One point, however, is specific to Leidenfrost drops, namely that the dynamics itself may perturb the Leidenfrost state (Celata et al. 2006, Wang et al. 2000). On the one hand, bouncing drops spend only a few milliseconds on the solid [the Rayleigh time  $(\rho R^3 / \gamma)^{1/2}$  of a deformation], so the nonstationary vapor film might be thinner than the scale of roughness. On the other hand, and more importantly, the impinging drop presses on the film (in construction) with a dynamic pressure  $\rho V^2$  much larger than the Laplace or hydrostatic pressure in a static case for  $We > 1$ . Hence dynamic levitation is more demanding than static levitation, and the Leidenfrost temperature  $T_L$  can be shifted to higher values and increase with  $We$  (Bernardin & Mudawar 2004, Tran et al. 2012, Yao & Cai 1988).

**Figure 8** shows a phase diagram of the different behaviors observed as water drops impact a hot plate (Tran et al. 2012). One phase observed is the film-boiling regime discussed in this review for

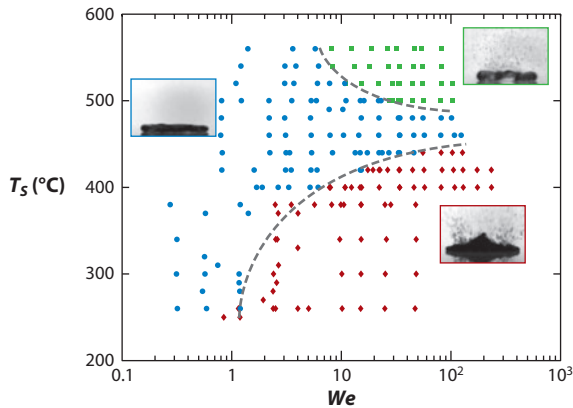


**Figure 8**

Phase diagram for the impact of water drops (surface tension  $\gamma$ , density  $\rho$ , radius  $R$ , and velocity  $V$ ) on hot plates (temperature  $T_S$ ). In a static case ( $We = 0$ ), the Leidenfrost temperature  $T_L$  is 160°C. For  $We = \rho V^2 R / \gamma > 1$ , three phases are observed: a contact-boiling regime (*red data*) at low temperature, below the dotted line; a film-boiling or Leidenfrost regime (*blue data*) at higher temperature; and a spraying-film-boiling regime (*green data*) at even higher  $T_S$ . Figure taken from Tran et al. (2012), courtesy of Tuan Tran and Detlef Lohse.

$T_S > T_L$  (**Supplemental Video 9**). The static value of  $T_L$  is 160°C for water on this surface, but for  $We > 1$ ,  $T_L$  impressively increases with  $We$  and reaches 400°C for  $We = 10$  (bottom dotted line in the figure). Below the line, the data show situations in which tiny droplets are ejected at impact (owing to the venting of vapor bubbles), revealing a contact between the liquid and the hot solid (**Supplemental Video 10**) (Ge & Fan 2005, Mehdizadeh & Chandra 2006). This ejection can be suppressed if polymers are present in the liquid (Bertola & Sefiane 2005). In addition, a third phase is observed in this regime of relatively high  $We$ : On very hot plates ( $T_S > 500^\circ\text{C}$ ), a spray forms above the spreading drop (see the inset in **Figure 8** and **Supplemental Video 11**), corresponding to the ejection of droplets from the top of the liquid. Experiments conducted in the film-boiling regime close to the boundary  $T_L(We)$  indicate that the vapor film is only a few micrometers in thickness, at least one order of magnitude thinner than expected at equilibrium (Tran et al. 2012), which is another way to stress the fragility of the Leidenfrost state in these dynamical situations. All these facts remain to be modeled, but they suggest that dynamical Leidenfrost situations can differ from the static (stationary) or quasi-static (slowly evaporating) cases reported above.

 Supplemental Material

### 3.3. Self-Propulsion

The frictionless character of Leidenfrost drops makes it possible to propel them at appreciable velocities with tiny forces. In this spirit, a remarkable achievement is the device proposed by Linke et al. (2006), who considered hot solids covered by asymmetric teeth (of depth  $a$  and size  $\lambda$ ) (**Figure 9**). It turns out that this pattern induces self-propulsion: The levitating liquid moves in the direction toward the steep side of the teeth and quickly reaches a final velocity of the order of  $10 \text{ cm s}^{-1}$  (Fenga et al. 2012, Lagubeau et al. 2011, Linke et al. 2006, Ok et al. 2011) (see **Supplemental Video 12**). This effect was exploited by Cousins et al. (2012), who built concentric ridges (each asymmetric in cross section) and thus achieved a modern version of Leidenfrost's spoon: Regardless of the place where a drop is deposited, after a few oscillations, it ends up at the center of the ridges.

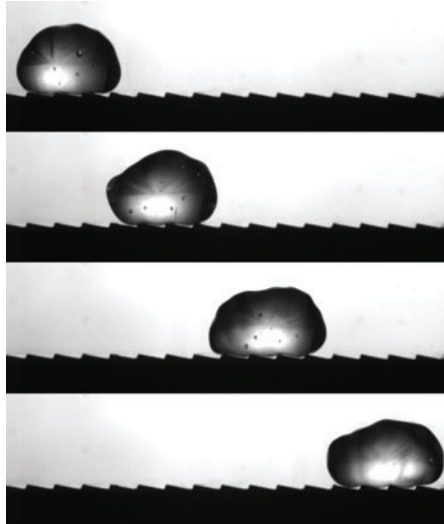


**Figure 9**

Linke's device. A liquid drop (of radius  $R = 2$  mm) is placed on a hot ratchet with teeth of depth  $a = 0.2$  mm and length  $\lambda = 1.5$  mm. For ratchet temperatures larger than  $T_L$ , the drop self-propels such that it hits the step (which is also the direction of maximal friction, as discussed in Section 3.1). The interval between successive pictures is 40 ms. Figure courtesy of Marie Le Merrer.

The force  $F$  acting on the liquid was measured and found to increase with the radius  $R$  and to be of the order of  $10 \mu\text{N}$  (again, small compared to the drop weight). **Figure 9** and **Supplemental Video 12** show waves propagating along the interface, small oscillations of the liquid, and deformations below (owing to the teeth, and similar to the ones in **Figure 6**), which all might contribute to a balance of forces. In this context, it is useful to realize that Leidenfrost solids (such as that shown in **Figure 1c**) also self-propel on hot ratchets in the same direction as liquids (Lagubeau et al. 2011). This observation shows that interfaces do not necessarily need to be deformable to obtain self-propulsion and rather designates the vapor flow as the cause of motion.

With regard to vapor ejection (discussed in Section 2.3), for large drops, the velocity  $U$  of the gas was found to be independent of the drop radius and of the order of  $10 \text{ cm s}^{-1}$ . The flow is isotropic if the Leidenfrost material levitates above a flat solid, but it can be rectified on asymmetric patterns, as shown in the context of flows against ratchets (Jiang et al. 1998, Yang et al. 2004). For thin films ( $b < a$ ), it was shown experimentally (using tracers) and numerically that the vapor flow is generally a lubrication flow (Cousins et al. 2012, Dupeux et al. 2011b), in which the gas is directed toward the deepest part of each tooth (**Supplemental Video 13**), then hits the step, and escapes laterally along it. Hence the pattern makes the vapor flow cellular (there is nearly no gas exchange between two successive teeth), and rectified, in the direction chosen by the levitating body: Owing to the vapor viscosity, this flow can drag the material above (Cousins et al. 2012, Dupeux et al. 2011b, Linke et al. 2006), which suggests a traction force  $F$  scaling as  $(\eta_v U/d)R^2$ , where  $d$  is a typical vapor thickness (between  $b$  and  $a$ ). This general formula gives correct orders of magnitude for  $F$  (typically  $10\text{--}100 \mu\text{N}$ ), and it explains the strong variation of  $F(R)$  observed experimentally, even if the details of this force are still discussed in the literature. Less plausible scenarios have also been proposed, such as thermal creep due to temperature gradients on the ratchet (this provides a very weak force at the macroscopic scale of the experiments shown in **Figure 9**) (Würger 2011) or the rocket effect (which assumes a gas flow rectified in the opposite

direction) (Lagubeau et al. 2011). The scenario of a viscous drag seems presently well established, which should lead to new kinds of self-propelling devices: Patterns forcing the vapor flow in a given direction should propel the levitating material in the same direction.

#### 4. CONCLUSION AND FUTURE DIRECTIONS

The Leidenfrost phenomenon contains and condenses many aspects of interfacial hydrodynamics. It implies two fluids, a vapor and liquid, which are both in motion: The vapor is fed by the evaporation of the liquid above, and it flows because of the pressure this liquid exerts on it; the liquid is subjected to internal motion and self-oscillations, and its swift displacements indicate a tiny friction, which itself can be exploited to create self-propelling devices. In addition, we have different interfaces, which all play a role. The solid/vapor interface at the surface of the hot solid provides a no-slip condition, and it can be textured to induce special properties (e.g., the nucleation of bubbles with fine textures, self-propulsion for asymmetric ones). At a liquid/vapor interface, molecule exchange takes place, and the interface's softness makes it possibly unstable (e.g., the formation of chimneys across the liquid). At a top liquid/air interface, the temperature can be different from the bottom one, generating Marangoni flows in the liquid. Owing to the different scales of the phases present, Leidenfrost drops compose a simple system in which viscous flows (mainly in the vapor gap) coexist with inertial flows (mainly in the drop)—hence there is a richness of behaviors in this spheroidal state (Bouasse 1924, Curzon 1978).

This richness has not been completely explored nor exploited. In addition to the remarks made above about possible extensions of current research, I stress two main future directions. First, ultramobile Leidenfrost drops are most often elusive, and controlling them can be crucial, in particular in applications in which they are used to drive heat away from a hot substrate. Above it is mentioned that crenulations can be used to slow and even trap liquid, and asymmetric teeth propel it in well-defined directions. Even if we restrict ourselves to a geometrical control, many other devices could be explored and quantified—for example, a simple groove on a solid can act as a rail for the liquid (Abbyad et al. 2011), and other asymmetric patterns should also yield self-propulsion. But control could be triggered by other kinds of fields: The actions of electric or magnetic fields on levitating drops have been described very little (Celestini & Kirstetter 2012, Piroird et al. 2012). Sensitivity to these fields may arise not only from the nature of the liquid, but also from particles dispersed in it—which raises the different and stimulating question of complex Leidenfrost states, such as Leidenfrost suspensions (Elbahri et al. 2007, Tsapis et al. 2005), solutions (Bertola & Sefiane 2005, Cui et al. 2003), mixtures (Chiu & Lin 2005), and gels. Second, this review considers the thermal Leidenfrost phenomenon, but the phenomenon may be extended to any system in which a film of gas is forced between a substrate and a liquid. This can be achieved using dynamics: A motion of the substrate, or along the liquid/vapor interface, can also feed the gas below the drop and possibly generate levitation. At least three examples of this kind have been published in the literature: Oil can bounce on a vibrating bath of the same oil (Couder et al. 2005, Protiere et al. 2006); a liquid hotter than its substrate can levitate because associated Marangoni flows in the liquid draw air with them, which feeds the film below (Nagy & Neitzel 2008, 2009; Neitzel & Dell'Aversana 2002); and a drop gently deposited on a plate or on a liquid moving at a high velocity can levitate on it, provided the plate moves fast enough (Pirat et al. 2010, Povarov et al. 1975, Sreenivas et al. 1999). These dynamical Leidenfrost states still need to be characterized quantitatively (e.g., phase diagram, robustness of the states) and compared to the thermal states described above. Despite the classicism of the Leidenfrost phenomenon, we can be confident 250 years after its discovery that this effect, which provides repellency and high liquid mobility, still has its best days ahead.

## DISCLOSURE STATEMENT

The author is not aware of any biases that might be perceived as affecting the objectivity of this review.

## ACKNOWLEDGMENTS

I frequently interacted with Christophe Clanet on these subjects, and it is a real pleasure to thank him for his constant and inspiring input. Anne-Laure Biance was our first PhD student working on Leidenfrost drops, and with Frédéric Chevy, she explored many aspects of their levitating life. Stimulated by the remarkable experiment of Heiner Linke, we recently started new programs in which Mathieu Bancelin, Baptiste Darbois, Guillaume Dupeux, Guillaume Lagubeau, Marie Le Merrer, Keyvan Piroird, Dan Soto, and Raphaële Thévenin participated actively. I also benefited from the help of and exchanged ideas with T. Baier, J.C. Bird, P. Brunet, J. Eggers, R.E. Goldstein, S. Hardt, J. Hinch, H. Linke, D. Lohse, L. Mahadevan, S.R. Nagel, G.P. Neitzel, K. Okumura, E. Raphael, J. Snoeijer, S.T. Thoroddsen, T. Tran, and I.U. Vakarelski. Jim Gibbons gave wonderful semantic advice. I am happy to warmly thank all of them.

## LITERATURE CITED

- Abbyad P, Dangla R, Alexandrou A, Baroud CN. 2011. Rails and anchors: guiding and trapping droplet microreactors in two dimensions. *Lab Chip* 11:813–21
- Adachi K, Takaki R. 1984. Vibration of a flattened drop: 1. Observation. *J. Phys. Soc. Jpn.* 53:4184–91
- Aussillous P, Quéré D. 2006. Properties of liquid marbles. *Proc. R. Soc. A* 462:973–99
- Avedisian CT, Koplik J. 1987. Leidenfrost boiling of methanol droplets on hot porous/ceramic surfaces. *Int. J. Heat Mass Transf.* 30:379–93
- Barthlott W, Neinhuis C. 1997. Purity of the sacred lotus, or escape from contamination in biological surfaces. *Planta* 202:1–8
- Bernardin JD, Mudawar I. 1997. Film boiling heat transfer of droplet streams and sprays. *Int. J. Heat Mass Transf.* 40:2579–93
- Bernardin JD, Mudawar I. 1999. The Leidenfrost point: experimental study and assessment of existing models. *J. Heat Transf.* 121:894–903
- Bernardin JD, Mudawar I. 2004. A Leidenfrost point model for impinging droplets and sprays. *J. Heat Transf.* 126:272–78
- Bernardin JD, Mudawar I. 2007. Transition boiling heat transfer of droplet streams and sprays. *J. Heat Transf.* 129:1605–10
- Bernardin JD, Stebbins CJ, Mudawar I. 1997a. Effects of surface roughness on water droplet impact history and heat transfer regimes. *Int. J. Heat Mass Transf.* 40:73–88
- Bernardin JD, Stebbins CJ, Mudawar I. 1997b. Mapping of impact and heat transfer regimes of water drops impinging on a polished surface. *Int. J. Heat Mass Transf.* 40:247–67
- Bertola V, Sefiane S. 2005. Controlling secondary atomization during drop impact on hot surfaces by polymer additives. *Phys. Fluids* 17:108104
- Biance AL, Chevy F, Clanet C, Lagubeau G, Quéré D. 2006. On the elasticity of an inertial liquid shock. *J. Fluid Mech.* 554:47–66
- Biance AL, Clanet C, Quéré D. 2003. Leidenfrost drops. *Phys. Fluids* 15:1632–37
- Biance AL, Pirat C, Ybert C. 2011. Drop fragmentation due to hole formation during Leidenfrost impact. *Phys. Fluids* 23:022104
- Bleiker G, Specht E. 2007. Film evaporation of drops of different shape above a horizontal plate. *Int. J. Therm. Sci.* 46:835–41
- Boerhaave H. 1732. *Elementae Chemiae*, Vol. 1. Leiden: Lugduni Batavorum
- Bouasse H. 1924. *Capillarité: Phénomènes Superficiels*. Paris: Delagrave

- Brunet P, Snoeijer JH. 2011. Star-drops formed by periodic excitation and on an air cushion: a short review. *Eur. Phys. J. Spec. Top.* 192:207–26
- Burton JC, Sharpe AL, van der Veen RCA, Franco A, Nagel SR. 2012. Geometry of the vapor layer under a Leidenfrost drop. *Phys. Rev. Lett.* 109:074301
- Celata GP, Cumo M, Mariani A, Zummo G. 2006. Visualization of the impact of water drops on a hot surface: effect of drop velocity and surface inclination. *Heat Mass Transf.* 42:885–90
- Celestini F, Frisch T, Pomeau Y. 2012. Take off of small Leidenfrost droplets. *Phys. Rev. Lett.* 109:034501
- Celestini F, Kirstetter G. 2012. Effect of an electric field on a Leidenfrost droplet. *Soft Matter* 8:5992–95
- Chandra S, Avedisian C. 1991. On the collision of a droplet with a solid surface. *Proc. R. Soc. A* 432:13–41
- Chiu SL, Lin TH. 2005. Experiment on the dynamics of a compound drop impinging on a hot surface. *Phys. Fluids* 17:122103
- Cossali GE, Marengo M, Santini M. 2008. Thermally induced secondary drop atomisation by single drop impact onto heated surfaces. *Int. J. Heat Fluid Flow* 29:167–77
- Couder Y, Fort E, Gautier CH, Boudaoud A. 2005. From bouncing to floating: noncoalescence of drops on a fluid bath. *Phys. Rev. Lett.* 94:177801
- Cousins TR, Goldstein RE, Jaworski JW, Pesci AI. 2012. A ratchet trap for Leidenfrost drops. *J. Fluid Mech.* 696:215–27
- Cui Q, Chandra S, McCahan S. 2003. The effect of dissolving salts in water sprays used for quenching a hot surface: part 2—spray cooling. *J. Heat Transf.* 125:333–38
- Curzon FL. 1978. The Leidenfrost phenomenon. *Am. J. Phys.* 46:825–28
- Dupeux G, Le Merrer M, Clanet C, Quéré D. 2011a. Trapping Leidenfrost drops with crenulations. *Phys. Rev. Lett.* 107:114503
- Dupeux G, Le Merrer M, Lagubeau G, Clanet C, Hardt S, Quéré D. 2011b. Viscous mechanism for Leidenfrost propulsion on a ratchet. *Eur. Phys. Lett.* 96:58001
- Elbahri M, Paretkar D, Hirman K, Jebil S, Adelung R. 2007. Anti-lotus effect for nanostructuring at the Leidenfrost temperature. *Adv. Mater.* 19:1262–66
- Faraday M. 1828. On the relation of water to hot polished surfaces. *Q. J. Sci. Lit. Arts* 1:221
- Fenga R, Zhaoa W, Wu X, Xuea Q. 2012. Ratchet composite thin film for low-temperature self-propelled Leidenfrost droplet. *J. Colloid Interface Sci.* 367:450–54
- Fletcher DF, Thyagaraja A. 1989. A mathematical model of melt water detonations. *Appl. Math. Model.* 13:339–47
- Ge Y, Fan LS. 2005. Three-dimensional simulation of impingement of a liquid droplet on a flat surface in the Leidenfrost regime. *Phys. Fluids* 17:027104
- Goldshnik MA, Khanin VM, Lugal VG. 1986. A liquid drop on an air cushion as an analogue of Leidenfrost boiling. *J. Fluid Mech.* 166:1–20
- Gottfried BS, Lee CJ, Bell KJ. 1966. Leidenfrost phenomenon: film boiling of liquid droplets on a flat plate. *Int. J. Heat Mass Transf.* 9:1167–72
- Gradeck M, Kouachi A, Boreau JL, Gardin P, Lebouché M. 2011. Heat transfer from a hot moving cylinder impinged by a planar subcooled water jet. *Int. J. Heat Mass Transf.* 54:5527–39
- Hall RS, Board SJ, Clare AJ, Duffey RB, Playle TS, Poole DH. 1969. Inverse Leidenfrost phenomenon. *Nature* 224:266–67
- Harvie DJE, Fletcher DF. 2001a. A hydrodynamic and thermodynamic simulation of droplet impacts on hot surfaces, part I: theoretical model. *Int. J. Heat Mass Transf.* 44:2633–42
- Harvie DJE, Fletcher DF. 2001b. A hydrodynamic and thermodynamic simulation of droplet impacts on hot surfaces, part II: validation and applications. *Int. J. Heat Mass Transf.* 44:2643–59
- Jiang XN, Zhou ZY, Huang XY, Li Y, Yang Y, Liu CY. 1998. Micronozzle/diffuser flow and its application to micro valveless pumps. *Sens. Actuators A* 70:81–87
- Karl A, Frohn A. 2000. Experimental investigation of interaction processes between droplets and hot walls. *Phys. Fluids* 12:785–96
- Karwa N, Gambaryan-Roisman T, Stephan P, Tropea C. 2011. A hydrodynamic model for subcooled liquid jet impingement at the Leidenfrost condition. *Int. J. Therm. Sci.* 50:993–1000

- Kim H, Buongiorno J, Hu LW, McKrell T. 2010. Nanoparticle deposition effects on the minimum heat flux point and quench front speed during quenching in water-based alumina nanofluids. *Int. J. Heat Mass Transf.* 53:1542–53
- Kim H, DeWitt G, McKrell T, Buongiorno J, Hu LW. 2009. On the quenching of steel and zircaloy spheres in water-based nanofluids with alumina, silica and diamond nanoparticles. *Int. J. Multiphase Flow* 35:427–38
- Kim H, Truong B, Buongiorno J, Hu LW. 2011. On the effect of surface roughness height, wettability, and nanoporosity on Leidenfrost phenomena. *Appl. Phys. Lett.* 98:083121
- Lagubeau G, Le Merrer M, Clanet C, Quéré D. 2011. Leidenfrost on a ratchet. *Nat. Phys.* 7:395–98
- Leidenfrost JG. 1756a. *De Aquae Communis Nonnullis Qualitatibus Tractatus*. Duisburg: Ovenius
- Leidenfrost JG. 1756b. On the fixation of water in diverse fire. Transl. C. Wares, 1966, in *Int. J. Heat Mass Transf.* 9:1153–66
- Linke H, Alema BJ, Melling LD, Taormina MJ, Francis MJ, et al. 2006. Self-propelled Leidenfrost droplets. *Phys. Rev. Lett.* 96:154502
- Lister JR, Thompson AB, Perriot A, Duchemin L. 2008. Shape and stability of axisymmetric levitated viscous drops. *J. Fluid Mech.* 617:167–85
- Liu G, Craig VSJ. 2010. Macroscopically flat and smooth superhydrophobic surfaces: heating induced transition up to the Leidenfrost temperature. *Faraday Discuss.* 146:141–51
- Mahadevan L, Pomeau Y. 1999. Rolling droplets. *Phys. Fluids* 11:2449–53
- Mehdizadeh NZ, Chandra S. 2006. Boiling during high-velocity impact of water droplets on a hot stainless steel surface. *Proc. R. Soc. A* 462:3115–31
- Moita AS, Moreira ALN. 2007. Drop impacts onto cold and heated rigid surfaces: morphological comparisons, disintegration limits and secondary atomization. *Int. J. Heat Fluid Flow* 28:735–52
- Myers TG, Charpin JPF. 2009. A mathematical model of the Leidenfrost effect on an axisymmetric droplet. *Phys. Fluids* 21:063101
- Nagy PT, Neitzel GP. 2008. Optical levitation and transport of microdroplets: proof of concept. *Phys. Fluids* 20:101703
- Nagy PT, Neitzel GP. 2009. Failure of thermocapillary-driven permanent nonwetting droplets. *Phys. Fluids* 21:112106
- Neitzel GP, Dell’Aversana P. 2002. Noncoalescence and nonwetting behavior of liquids. *Annu. Rev. Fluid Mech.* 34:267–89
- Ok JT, Lopez-Onna E, Nikitopoulos DE, Wong H, Park S. 2011. Propulsion of droplets on micro- and sub-micron ratchet surfaces in the Leidenfrost temperature regime. *Microfluid. Nanofluid.* 10:1045–54
- Ou J, Perot B, Rothstein JP. 2004. Laminar drag reduction in microchannels using ultrahydrophobic surfaces. *Phys. Fluids* 16:4635–43
- Perrard S, Couder Y, Fort E, Limat L. 2012. Large Leidenfrost levitated liquid tori: stability and instabilities. Submitted manuscript
- Pirat C, Lebon L, Fruleux A, Roche JS, Limat L. 2010. Gyroscopic instability of a drop trapped inside an inclined circular hydraulic jump. *Phys. Rev. Lett.* 105:084503
- Piroird K, Clanet C, Quere D. 2012. Magnetic control of Leidenfrost drops. *Phys. Rev. E* 85:056311
- Povarov OA, Shalnev KK, Nazarov OI, Shalobasov IA. 1975. Collision of a drop with moving plane surface. *Dokl. Akad. Nauk SSSR* 225:553–56
- Protiere S, Boudaoud A, Couder Y. 2006. Particle-wave association on a fluid interface. *J. Fluid Mech.* 554:85–108
- Proust M. 1913. *Du côté de chez Swann*. Transl. L. Davis, 2003, in *Swann’s Way*. New York: Viking
- Snezhko A, Ben Jacob E, Aranson IS. 2008. Pulsating-gliding transition in the dynamics of levitating liquid nitrogen droplets. *New J. Phys.* 10:043034
- Snoeijer JH, Andreotti B. 2013. Moving contact lines: scales, regimes and dynamical transitions. *Annu. Rev. Fluid Mech.* 45:269–92
- Snoeijer JH, Brunet P, Eggers J. 2009. Maximum size of drops levitated by an air cushion. *Phys. Rev. E* 79:036307
- Song YS, Adler D, Xu F, Kayaalp E, Nureddin A, et al. 2010. Vitrification and levitation of a liquid droplet on liquid nitrogen. *Proc. Natl. Acad. Sci. USA* 107:4596–600

- Sreenivas KR, De PK, Arakeri JH. 1999. Levitation of a drop over a film flow. *J. Fluid Mech.* 380:297–307
- Strier DE, Duarte AA, Ferrari H, Mindlin GB. 2000. Nitrogen stars: morphogenesis of a liquid drop. *Physica A* 283:261–66
- Strotos G, Gavaises M, Theodorakakos A, Bergeles G. 2008. Numerical investigation on the evaporation of droplets depositing on heated surfaces at low Weber numbers. *Int. J. Heat Mass Transf.* 51:1516–29
- Takaki R, Adachi K. 1985. Vibration of a flattened drop: 2. Normal mode analysis. *J. Phys. Soc. Jpn.* 54:2462–69
- Taylor GI. 1950. The instability of liquid surfaces when accelerated in a direction perpendicular to their planes. *Proc. R. Soc. Lond. A* 201:192–96
- Tokugawa N, Takaki R. 1994. Mechanism of self-induced vibration of a liquid drop based on the surface tension fluctuation. *J. Phys. Soc. Jpn.* 63:1758–68
- Tong LS. 1997. *Boiling Heat Transfer and Two-Phase Flow*. Philadelphia: Taylor & Francis
- Tran T, Staat HJJ, Prosperetti A, Sun C, Lohse D. 2012. Drop impact on superheated surfaces. *Phys. Rev. Lett.* 108:036101
- Tsapis N, Dufresne ER, Sinha SS, Riera CS, Hutchinson JW, et al. 2005. Onset of buckling in drying droplets of colloidal suspensions. *Phys. Rev. Lett.* 94:018302
- Vakarelski IU, Marston JO, Chan DYC, Thoroddsen ST. 2011. Drag reduction by Leidenfrost vapor layers. *Phys. Rev. Lett.* 106:214501
- Vakarelski IU, Patankar NA, Marston JO, Chan DYC, Thoroddsen ST. 2012. Stabilization of Leidenfrost vapour layer by textured superhydrophobic surfaces. *Nature* 489:274–77
- Verne J. 1876. *Michel Strogoff*. Paris: Hetzel
- Wachters LHJ, Bonne H, van Nouhuis HJ. 1966. The heat transfer from a horizontal plate to sessile water drops in the spheroidal state. *Chem. Eng. Sci.* 21:923–30
- Wachters LHJ, Westerling NAJ. 1966. The heat transfer from a hot plate to impinging water drops in the spheroidal state. *Chem. Eng. Sci.* 21:1047–56
- Wang AB, Lin CH, Chen CC. 2000. The critical temperature of dry impact for tiny droplet impinging on a heated surface. *Phys. Fluids* 12:1622–25
- Weickgenannt CM, Zhang Y, Sinha-Ray S, Roisman IV, Gambaryan-Roisman T, et al. 2011. Inverse-Leidenfrost phenomenon on nanofiber mats on hot surfaces. *Phys. Rev. E* 84:036310
- Würger A. 2011. Leidenfrost gas ratchets driven by thermal creep. *Phys. Rev. Lett.* 107:164502
- Yang KS, Chen IY, Shew BY, Wang CC. 2004. Investigation of the flow characteristics within micronozzle/diffuser. *J. Micromech. Microeng.* 14:26–31
- Yao SC, Cai KY. 1988. The dynamics and Leidenfrost temperature of drops impacting on a hot surface at small angles. *Exp. Therm. Fluid. Sci.* 1:363–71
- Young T. 1805. An essay on the cohesion of fluids. *Philos. Trans. R. Soc. A* 95:65–87



# Contents

Hans W. Liepmann, 1914–2009 <i>Roddam Narasimha, Anatol Roshko, and Morteza Gharib</i> .....	1
Philip G. Saffman <i>D.I. Pullin and D.I. Meiron</i> .....	19
Available Potential Energy and Exergy in Stratified Fluids <i>Rémi Tailleux</i> .....	35
The Fluid Dynamics of Tornadoes <i>Richard Rotunno</i> .....	59
Nonstandard Inkjets <i>Osman A. Basaran, Haijing Gao, and Pradeep P. Bhat</i> .....	85
Breaking Waves in Deep and Intermediate Waters <i>Marc Perlin, Wooyoung Choi, and Zbigang Tian</i> .....	115
Balance and Spontaneous Wave Generation in Geophysical Flows <i>J. Vanneste</i> .....	147
Wave Packets and Turbulent Jet Noise <i>Peter Jordan and Tim Colonius</i> .....	173
Leidenfrost Dynamics <i>David Quéré</i> .....	197
Ice-Sheet Dynamics <i>Christian Schoof and Ian Hewitt</i> .....	217
Flow in Foams and Flowing Foams <i>Sylvie Cohen-Addad, Reinhard Höbler, and Olivier Pitois</i> .....	241
Moving Contact Lines: Scales, Regimes, and Dynamical Transitions <i>Jacco H. Snoeijer and Bruno Andreotti</i> .....	269
Growth of Cloud Droplets in a Turbulent Environment <i>Wojciech W. Grabowski and Lian-Ping Wang</i> .....	293
The Fluid Mechanics of Cancer and Its Therapy <i>Petros Koumoutsakos, Igor Pivkin, and Florian Milde</i> .....	325

Analysis of Fluid Flows via Spectral Properties of the Koopman Operator <i>Igor Mezić</i> .....	357
The Interaction of Jets with Crossflow <i>Krishnan Mabesh</i> .....	379
Particle Image Velocimetry for Complex and Turbulent Flows <i>Jerry Westerweel, Gerrit E. Elsinga, and Ronald J. Adrian</i> .....	409
Fluid Dynamics of Human Phonation and Speech <i>Rajat Mittal, Byron D. Erath, and Michael W. Plesniak</i> .....	437
Sand Ripples and Dunes <i>François Charru, Bruno Andreotti, and Philippe Claudin</i> .....	469
The Turbulent Flows of Supercritical Fluids with Heat Transfer <i>Jung Yul Yoo</i> .....	495

## Indexes

Cumulative Index of Contributing Authors, Volumes 1–45 .....	527
Cumulative Index of Chapter Titles, Volumes 1–45 .....	536

## Errata

An online log of corrections to *Annual Review of Fluid Mechanics* articles may be found at <http://fluid.annualreviews.org/errata.shtml>